Instability in gravity-driven flow over uneven surfaces

S. J. D. D'Alessio,[1,a)] J. P. Pascal,[2,b)] and H. A. Jasmine[2,c)]
[1]*Department of Applied Mathematics, University of Waterloo, Waterloo, Ontario N2L 3G1, Canada*
[2]*Department of Mathematics, Ryerson University, Toronto, Ontario M5B 2K3, Canada*

(Received 18 January 2009; accepted 22 May 2009; published online 17 June 2009)

We consider the gravity-driven laminar flow of a shallow fluid layer down an uneven incline with the principal objective of investigating the effect of bottom topography and surface tension on the stability of the flow. The equations of motion are approximations to the Navier–Stokes equations which exploit the assumed relative shallowness of the fluid layer. Included in these equations are diffusive terms that are second order relative to the shallowness parameter. These terms, while small in magnitude, represent an important dependence of the flow dynamics on the variation in bottom topography and play a significant role in theoretically capturing important aspects of the flow. Some of the second-order terms include normal shear contributions, while others lead to a nonhydrostatic pressure distribution. The explicit dependence on the cross-stream coordinate is eliminated from the equations of motion by means of a weighted residual approach. The resulting mathematical formulation constitutes an extension of the modified integral-boundary-layer equations proposed by Ruyer-Quil and Manneville [Eur. Phys. J. B **15**, 357 (2000)] for flows over even surfaces to flows over variable topography. A linear stability analysis of the steady flow is carried out by taking advantage of Floquet–Bloch theory. A numerical scheme is devised for solving the nonlinear governing equations and is used to calculate the evolution of the perturbed equilibrium flow. The simulations are used to confirm the analytical predictions and to investigate the interfacial wave structure. The bottom profile considered in this investigation corresponds to periodic undulations characterized by measures of wavelength and amplitude. Conclusions are drawn on the combined effect of bottom topography and surface tension. © *2009 American Institute of Physics*.
[DOI: 10.1063/1.3155521]

I. INTRODUCTION

The instability of free-surface flow down an incline results in the formation of large-amplitude interfacial waves propagating with a permanent shape and speed. The appearance of such a wave pattern on the surface of the fluid layer is generally associated with undesired consequences be it in the natural environment or industrial settings. In man-made conduits such as open aqueducts, spillways of dams, and runoff channels, the flow instability generates a series of intermittent bores commonly referred to as "roll waves." These surges can damage flow control and flow measuring devices and can even raise the fluid level above the channel walls. In naturally occurring debris flows surface bores can drastically increase their destructive power. Interfacial instabilities exhibited by gravity-driven film flows can have an important impact in various technological applications such as coating operations connected to manufacturing processes. The detrimental effects of hydrodynamic instability can potentially be reduced or possibly eliminated by capitalizing on theoretical predictions of flow behavior. A mathematical model can be used to anticipate the conditions under which a simple steady discharge will ultimately become unstable and develop interfacial waves.

To accurately represent an unsteady and nonuniform flow arising from interfacial instability, a mathematical model must incorporate all the relevant physical factors and possess the mathematical complexity required to capture the spatiotemporal coupling and nonlinear dynamics of the flow. At the same time, simplifications to the governing equations, warranted by physically justified assumptions, can lead to a more complete and productive mathematical treatment. A general modeling approach is to reduce the space dimensionality of the problem by relying on the assumed shallowness of the flow and effectuating a depth integration of the equations of motion. The success of this strategy requires that the velocity variation with depth be consistent with laminar flow and be specified *a priori*. A suitable approximation can be constructed from the self-similar parabolic velocity profile produced by the balance between gravity and longitudinal shear which governs the steady and uniform flow. Fitting the profile to the boundary conditions at the top and bottom of the fluid layer introduces dependence on the thickness of the layer which is transient and nonuniform for unstable flows. The resulting equations governing the thickness and flow rate of the fluid layer are referred to as integral-boundary-layer (IBL) equations.

These equations turn out to be quite effective in capturing the behavior of the flow under supercritical conditions. Alekseenko *et al.*[1] confirmed by direct measurements that the parabolic velocity profile assumed in the IBL approach accurately describes the flow in the nonuniform and transient regime. Julien and Hartley[2] have found the celerity of roll

[a)]Electronic mail: sdalessio@uwaterloo.ca.
[b)]Electronic mail: jpascal@ryerson.ca.
[c)]Electronic mail: hjasmine@ryerson.ca.

waves determined by the IBL theory to be in good agreement with measurements from their experimental setup. It must be mentioned, however, that the IBL model overestimates the critical conditions for the onset of instability as compared to the results from the Orr–Sommerfeld equations[3,4] and the experimental work reported by Liu *et al.*[5]

The original and most commonly used form of the IBL equations was established by Shkadov.[6] These equations have first-order status since they originate from the Navier–Stokes equations simplified by the removal of $O(\delta^2)$ terms and higher, where δ is the shallowness parameter. A more accurate second-order form of the IBL equations was first proposed by Prokopiou *et al.*[7] However, their derivation is based on the assumption of a hydrostatic pressure distribution which is known to be consistent with only a first-order approximation. Uecker[8] used a formal scaling of the Navier–Stokes equations to identify and discard terms of $O(\delta^3)$ and higher. This approximation to the Navier–Stokes equations contains second-order terms which introduce nonhydrostatic effects in the subsequent IBL equations. In spite of this, the equations make the same erroneous predictions for the onset of instability as their first-order counterpart.

Ruyer-Quil and Manneville[9] also started with the second-order approximation to the Navier–Stokes equations but their integrated equations are obtained by considering a more accurate velocity profile obtained by means of a weighted residual technique with a polynomial expansion for the velocity. The model derived by Ruyer-Quil and Manneville correctly predicts the critical conditions for the onset of linear instability. Furthermore, it captures the development of the supercritical flow as revealed by comparison with the laboratory experiments of Liu *et al.*[10] and the direct numerical simulations conducted by Ramaswamy *et al.*[11] The ability of this model to accurately describe flows under unstable conditions far from criticality qualifies it as an important improvement over Benney's equation[12] which is only effective under conditions near the instability threshold.

Extending a model for inclined flow to account for bottom topography serves to widen its range of physical applications. In describing film flows, this extension will enable the model to capture the potential unevenness of the substrate. Film flows usually remain laminar mostly as a consequence of the low flow rates associated with their extreme thinness. The laminar flow assumption can also be made for shallow flows with a more substantial depth due to a reduced inclination or the material properties of the fluid. Debris flows, for example, can be laminar in spite of their fast rate of flow due to their high viscosity or their constitutive makeup. Hunt[13] reported that descriptions of debris flows obtained via a Newtonian laminar model are consistent with field observations and laboratory data. Ng and Mei[14] concentrated specifically on mud flows and provided further evidence of the laminar nature of these flows.

For environmental flows bottom unevenness can be associated with a naturally rugged terrain or the presence of rills formed as a result of soil erosion.[15] If the flow is to follow an artificial channel, then the intentional construction of a conduit with an uneven bottom can prevent the onset of flow instability.[16]

An evident possibility in constructing an appropriate model for flow over uneven topography is to consider an inclined surface exhibiting periodic undulations parametrized by measures of amplitude and wavelength. This approach was taken by Trifonov[17] in studying the steady laminar flow of thin films falling down a vertical wavy wall. He employed a spectral method to obtain numerical approximations to the Navier–Stokes equations as well as the first-order IBL equations. An investigation of the steady flow has recently been carried out by Heining *et al.*[18] who examined nonlinear resonance in gravity-driven flows along undulating surfaces with arbitrary inclination.

The stability of flow over uneven topography was first considered by Tougou[19] who conducted a weakly nonlinear analysis of inclined flow over a weakly wavy bottom and derived a Kuromoto–Sivashinsky-type equation incorporating the bottom unevenness. His analysis was later extended by Usha and Uma[20] to the viscoelastic fluid case. Davalos-Orozco[21] utilized a Benney-type equation to analyze Newtonian flow down a vertical wall with smooth corrugations.

Wierschem *et al.*[22] investigated the flow along a wavy inclined surface by considering a perturbation analysis of the Navier–Stokes equations with respect to a thin-film parameter. Under the assumptions of long bottom undulations, weak surface tension, and Reynolds numbers of order 1, the steady flow is approximated by a perturbation expansion about the uniform flow that would occur in the absence of the small bottom irregularities. The results of a linear stability analysis are confirmed by experimental findings and indicate that bottom topography has a stabilizing effect on the steady flow. The same general conclusion was reported by Vlachogiannis and Bontozoglou[23] from their experiments of flows over corrugated surfaces. Trifonov[24] used the first-order IBL equations to study the stability of film flow down an uneven vertical wall. In a later paper[25] he compared these results with those obtained from a linear analysis of the Navier–Stokes equations carried out by means of a numerical algorithm based on a spectral method involving expansions in Chebyshev polynomials as functions of the cross-flow variable. A spectral method was also employed by Khayat and Kim[26] to deal with the cross-flow variation in the first-order boundary-layer equations governing viscoelastic flow falling down an uneven vertical surface. Recently, Oron and Heining[27] have investigated film flow falling on a corrugated periodic vertical wall by implementing a mathematical model based on the first-order weighted residual method proposed by Ruyer-Quil and Manneville.[9] In contrast to the previous investigations based on approximate solutions of the Navier–Stokes equations, the reduced spatial dimensionality of this model allows for a more efficient analytical and numerical investigation.

A stability analysis of shallow flow along an uneven surface of small, yet arbitrary inclination has been reported by Balmforth and Mandre.[28] They employed the shallow-water equations enhanced with the empirical term for turbulent friction contributed by Dressler[29] and the internal dissipation term proposed by Needham and Merkin.[30] Bottom topography is introduced into the equations through the longitudinal

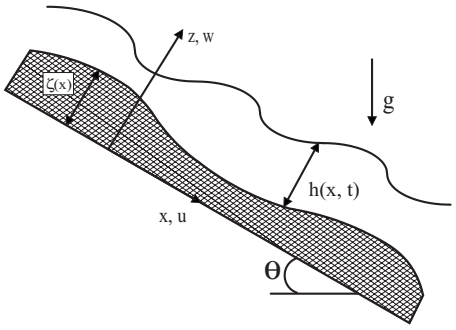

FIG. 1. The flow configuration.

gradient of the hydrostatic pressure. The empirical nature of the internal dissipation term forced Balmforth and Mandre to use a formulation that is independent of the bottom configuration. As part of their investigation, Balmforth and Mandre also considered a separate model for laminar flow. However, the equations are not methodically derived and rely on the same empirical internal dissipation term that is added to the shallow-water equations. As is pointed out by Prokopiou, *et al.*,[7] both periodic and solitary wave solutions to the shallow-water equations modified with this dissipative term display amplitudes that are strongly dependent on the viscosity coefficient. Consequently, it becomes very difficult to appropriately estimate this parameter.

In the present work we derive and implement a model for laminar flow over an inclined surface exhibiting periodic undulations. The model includes inertial and surface tension effects as well as important second-order diffusive terms. The bottom topography is methodically introduced into the equations resulting in second-order terms that are strongly dependent on the local steepness of the bottom profile. We obtain equations governing the depth and local flow rate in the fluid layer by following a weighted residual approach proposed by Ruyer-Quil and Manneville.[9] This derivation is outlined in Sec. II. In Sec. III a linear stability analysis is effectuated, while in Sec. IV a numerical method for solving the nonlinear equations is described. The numerical scheme is capable of calculating the entire evolution of a perturbed equilibrium. The results serve to verify the predictions of the analytical approach and also provide a description of the interfacial wave patterns arising from unstable flows. Lastly, a summary is included in Sec. V.

II. GOVERNING EQUATIONS

We consider the two-dimensional laminar flow of a shallow layer of a Newtonian fluid along an uneven inclined surface as shown in Fig. 1. We define an (x,z) coordinate system with the x-axis inclined at an angle θ with respect to the horizontal and pointing in the downhill direction and with the z-axis pointing in the upward normal direction. The surface over which the fluid is flowing is assumed to consist of periodic undulations expressed by

$$z = \zeta(x) = A_b \cos\left(\frac{2\pi x}{\lambda_b}\right),$$

with the parameters A_b and λ_b characterizing the amplitude and wavelength of the undulations, respectively. The fluid velocity is denoted by $\mathbf{u}=(u,w)^T$.

In scaling the equations of motion, for the vertical length scale we employ the Nusselt thickness H resulting from a constant discharge Q, which is given by

$$H = \left(\frac{3\ \mu Q}{\rho g \sin\theta}\right)^{1/3},$$

where g is the acceleration due to gravity and ρ,μ are the fluid density and viscosity, respectively. The pressure is scaled using ρU^2, where $U=Q/H$ is the velocity scale. The corresponding time scale is taken to be l/U, where l is the horizontal length scale. An obvious choice for the horizontal length scale is $l=\lambda_b$.

The governing two-dimensional Navier–Stokes equations can then be rendered in the following dimensionless form:

$$\frac{\partial u}{\partial x} + \frac{\partial w}{\partial z} = 0, \tag{1}$$

$$\delta\,\mathrm{Re}\frac{Du}{Dt} = -\,\delta\,\mathrm{Re}\frac{\partial p}{\partial x} + 3 + \delta^2\frac{\partial^2 u}{\partial x^2} + \frac{\partial^2 u}{\partial z^2}, \tag{2}$$

$$\delta^2\,\mathrm{Re}\frac{Dw}{Dt} = -\,\mathrm{Re}\frac{\partial p}{\partial z} - 3\cot\theta + \delta^3\frac{\partial^2 w}{\partial x^2} + \delta\frac{\partial^2 w}{\partial z^2}, \tag{3}$$

where D/Dt denotes the two-dimensional material derivative, $\delta=H/l=H/\lambda_b$ is the shallowness parameter, and $\mathrm{Re}=\rho Q/\mu$ is the Reynolds number.

In this investigation we focus on the instability of inclined flows that are sufficiently steep to become unstable at Reynolds numbers of $O(1)$. Therefore, we assume that Re is of $O(1)$ and, consequently, discarding the terms of $O(\delta^3)$ and higher in Eqs. (1)–(3) we obtain

$$\frac{\partial u}{\partial x} + \frac{\partial w}{\partial z} = 0, \tag{4}$$

$$\delta\,\mathrm{Re}\frac{Du}{Dt} = -\,\delta\,\mathrm{Re}\frac{\partial p}{\partial x} + 3 + \delta^2\frac{\partial^2 u}{\partial x^2} + \frac{\partial^2 u}{\partial z^2}, \tag{5}$$

$$\delta^2\,\mathrm{Re}\frac{Dw}{Dt} = -\,\mathrm{Re}\frac{\partial p}{\partial z} - 3\cot\theta + \delta\frac{\partial^2 w}{\partial z^2}. \tag{6}$$

As it is also specified by Ruyer-Quil and Manneville,[31] the inertia term on the left-hand side of the z-momentum equation (6) in actuality only offers a third-order contribution. This becomes evident once the pressure is eliminated from the x-momentum equation. As a result then, neglecting the inertia term in Eq. (6) leads to a second-order model for flows with Reynolds numbers of $O(1)$.

Assuming no external forcing at the surface of the fluid layer, the dynamic conditions become

$$0 = \delta^2\,\mathrm{We}\left(1+\delta^2\left[\frac{\partial z_1}{\partial x}\right]^2\right)^{-3/2}\frac{\partial^2 z_1}{\partial x^2} + p - \frac{2}{\mathrm{Re}}\left(1+\delta^2\left[\frac{\partial z_1}{\partial x}\right]^2\right)^{-1} \times\left(\delta^3\left[\frac{\partial z_1}{\partial x}\right]^2\frac{\partial u}{\partial x}+\delta\frac{\partial w}{\partial z}-\delta\frac{\partial z_1}{\partial x}\frac{\partial u}{\partial z}-\delta^3\frac{\partial z_1}{\partial x}\frac{\partial w}{\partial x}\right), \quad (7)$$

$$0 = \left(1-\delta^2\left[\frac{\partial z_1}{\partial x}\right]^2\right)\left(\frac{\partial u}{\partial z}+\delta^2\frac{\partial w}{\partial x}\right)-4\delta^2\frac{\partial z_1}{\partial x}\frac{\partial u}{\partial x}, \quad (8)$$

where $z_1=\zeta(x)+h(x,t)$ denotes the free surface and $\mathrm{We}=TH/(\rho Q^2)$ is the Weber number with T referring to the surface tension of the fluid.

We note that the surface tension term in Eq. (7) is of second order or larger if the Weber number is $O(1/\delta)$ or larger. Also, the term in Eq. (7) containing the z derivative of u is of $O(\delta^3)$ since the derivative itself is of $O(\delta^2)$ as is evident from Eq. (8). Therefore, to $O(\delta^3)$ the conditions at the surface of the fluid layer can be expressed as

$$\left.\begin{aligned} p-\frac{2\delta}{\mathrm{Re}}\frac{\partial w}{\partial z}+\delta^2\,\mathrm{We}\frac{\partial^2 z_1}{\partial x^2}&=0\\ \frac{\partial u}{\partial z}-4\delta^2\frac{\partial z_1}{\partial x}\frac{\partial u}{\partial x}+\delta^2\frac{\partial w}{\partial x}&=0\end{aligned}\right\} \quad \text{at } z=z_1. \quad (9)$$

The kinematic condition for the unknown surface position is expressed as

$$w=\frac{\partial h}{\partial t}+u\frac{\partial h}{\partial x}+u\zeta'(x),$$

and the scaled bottom profile is

$$\zeta(x)=a_b\cos(2\pi x), \quad \text{where } a_b=\frac{A_b}{H}=\frac{1}{\delta}\frac{A_b}{\lambda_b}.$$

In this study we will consider small bottom waviness having A_b/λ_b of $O(\delta)$ and thus a_b will be of $O(1)$.

At the interface between the fluid layer and the impermeable bottom the tangential and normal fluid velocity components are zero. Thus, we have

$$u+\zeta'(x)w=0 \quad \text{and} \quad \zeta'(x)u-w=0 \quad \text{at } z=\zeta(x),$$

and as a result we obtain the no-slip conditions

$$u=w=0 \quad \text{at } z=\zeta(x). \quad (10)$$

The fundamental premise that the flow under consideration is of small aspect ratio and slowly varying in the longitudinal direction warrants a depth averaging of the equations of motion. The subsequent elimination of the cross-flow variation results in a one-dimensional problem which is amenable to various mathematical analyses. Depth integrating the continuity equation (4) and incorporating the kinematic condition yields

$$\frac{\partial h}{\partial t}+\frac{\partial q}{\partial x}=0, \quad (11)$$

where the flow rate q is given by

$$q=\int_{\zeta(x)}^{\zeta(x)+h} u\,dz.$$

Integrating Eq. (6) from $z=z_1=h+\zeta$ to z and substituting the value for the pressure at the surface from the first condition in Eq. (9) provides the following expression for the total pressure:

$$p=\frac{3\cot\theta}{\mathrm{Re}}(z_1-z)-\frac{\delta}{\mathrm{Re}}\left.\frac{\partial u}{\partial x}\right|_{z=z_1}-\frac{\delta}{\mathrm{Re}}\frac{\partial u}{\partial x}-\delta^2\,\mathrm{We}\frac{\partial^2 z_1}{\partial x^2}-\delta^2\int_{z_1}^{z}\frac{Dw}{Dt}dz.$$

This can be used to eliminate the pressure from the x–momentum equation (5). However, due to the factor of δ multiplying the pressure gradient in Eq. (5), for $\mathrm{Re}\sim O(1)$ the integrated inertia term amounts to a third-order contribution in δ and can thus be discarded. This inertia term was retained by Lee and Mei[32] in their investigation of flows with Reynolds numbers of $O(1/\delta)$ down even inclines. If bottom unevenness is considered, including this term would complicate the equations considerably and hence limit the analysis. For this reason we restrict our investigation to Reynolds numbers of $O(1)$.

For the even bottom case, Ruyer-Quil and Manneville[9] have eliminated the explicit depth-coordinate dependence from the longitudinal momentum equation by implementing a weighted residual technique consisting of an expansion of the velocity field in terms of three suitably constructed polynomial functions. The complexity of the resulting system of equations, however, restricts the usefulness of the model. The authors consequently propose an approximation which simplifies the system to one consisting of two equations governing h and q referred to as the modified IBL equations. Ruyer-Quil and Manneville[33] found that this simplified model is quite effective in predicting the onset and evolution of interfacial instability. They demonstrate that the modified IBL model correctly predicts the critical conditions for the onset of linear instability. Further, the description of the nonlinear development of waves up to relatively high Reynolds numbers is in agreement with the experimental observations reported by Liu *et al.*[10] and the direct numerical simulations carried out by Ramaswamy *et al.*[11]

It turns out that the modified IBL equations can also be formally derived by applying the weighted residual method and using only one term in the spectral approximation of the velocity field. We now follow this approach in order to extend the modified IBL equations to the uneven bottom case. We begin by assuming the velocity to be of the form

$$u = \frac{3q}{2h^3} b,$$

where b is given by

$$b = 2(h + \zeta(x))z - z^2 - \zeta(x)^2 - 2\zeta(x)h,$$

and is to be viewed as the basis function in an expansion relative to the z dependence. In accordance with the Galerkin approach where b is also utilized as the weight function, we multiply Eq. (5) by b and integrate with respect to z from $\zeta(x)$ to $h+\zeta(x)$ to obtain the following dimensionless equations for the flow variables h and q:

$$\frac{\partial h}{\partial t} + \frac{\partial q}{\partial x} = 0, \tag{12}$$

$$\begin{aligned}
&\frac{\partial q}{\partial t} + \frac{9}{7}\frac{\partial}{\partial x}\left(\frac{q^2}{h}\right) \\
&\quad = \frac{q}{7h}\frac{\partial q}{\partial x} + \frac{5}{2\delta\,\mathrm{Re}}\left(h - \frac{q}{h^2}\right) - \frac{5\cot\theta}{2\,\mathrm{Re}} h\left(\frac{\partial h}{\partial x} + \zeta'\right) \\
&\qquad + \frac{5}{6}\delta^2\,\mathrm{We}\, h\left(\frac{\partial^3 h}{\partial x^3} + \zeta'''\right) + \frac{\delta}{\mathrm{Re}} \\
&\qquad \times \left[\frac{9}{2}\frac{\partial^2 q}{\partial x^2} - \frac{9}{2h}\frac{\partial q}{\partial x}\frac{\partial h}{\partial x} + \frac{4q}{h^2}\left(\frac{\partial h}{\partial x}\right)^2 - \frac{6q}{h}\frac{\partial^2 h}{\partial x^2}\right. \\
&\qquad \left. - \frac{5\zeta' q}{2h^2}\frac{\partial h}{\partial x} - \frac{15\zeta'' q}{4h} - \frac{5(\zeta')^2 q}{h^2}\right].
\end{aligned} \tag{13}$$

Setting $\zeta(x) \equiv 0$ corresponds to the even bottom case and reduces Eqs. (12) and (13) to the second-order modified IBL equations of Ruyer-Quil and Manneville.[9] In the general case, the terms in the last two lines of Eq. (13) capture the coupling of the second-order diffusive terms and the effect of bottom topography.

III. LINEAR STABILITY ANALYSIS

From Eq. (12) we obtain that the steady-state solution for q is a constant. If we use this constant as the discharge scale Q, then in dimensionless form we have that $q=q_s=1$ and $h=h_s(x)$, where $h_s(x)$ satisfies the nonlinear differential equation given by

$$\begin{aligned}
&\frac{5}{6}\delta^2\,\mathrm{We}\, h_s^3 h_s''' - \frac{2\delta}{\mathrm{Re}}[3h_s h_s'' - 2(h_s')^2] \\
&\quad - \left(\frac{5\cot\theta}{2\,\mathrm{Re}} h_s^3 + \frac{5\delta}{2\,\mathrm{Re}}\zeta' - \frac{9}{7}\right) h_s' - \frac{15\delta}{4\,\mathrm{Re}}\zeta'' h_s \\
&\quad + \left(\frac{5}{2\delta\,\mathrm{Re}} - \frac{5\cot\theta}{2\,\mathrm{Re}}\zeta' + \frac{5}{6}\delta^2\,\mathrm{We}\,\zeta'''\right) h_s^3 \\
&\quad = \frac{5}{2\delta\,\mathrm{Re}} + \frac{5\delta}{\mathrm{Re}}(\zeta')^2,
\end{aligned} \tag{14}$$

with the prime denoting differentiation with respect to x and once again $\zeta(x)=a_b\cos(2\pi x)$. For small δ an approximate analytical solution to Eq. (14) can be constructed in the form of a series given by

$$h_s(x) = 1 + \delta h_1(x) + \delta^2 h_2(x) + O(\delta^3).$$

Otherwise, $h_s(x)$ must be determined by numerically solving Eq. (14) over the computational domain $0 \le x \le 1$ subject to periodic boundary conditions. It is a straightforward exercise to verify that

$$h_1(x) = \tfrac{1}{3}\cot\theta\,\zeta'(x),$$

$$\begin{aligned}
h_2(x) &= \tfrac{2}{3}[\zeta'(x)]^2 + \tfrac{1}{2}\zeta''(x) - \tfrac{2}{35}\mathrm{Re}\cot\theta\,\zeta''(x) \\
&\quad + \tfrac{1}{9}\cot^2\theta(\zeta''(x) + 2[\zeta'(x)]^2).
\end{aligned}$$

To study how small disturbances will evolve when superimposed on the steady equilibrium solution, we linearize the governing equations by introducing perturbations $\hat{h}, \hat{q}$ and setting

$$h = h_s(x) + \hat{h}, \quad q = 1 + \hat{q}.$$

The linearized perturbation equations can then be written in the form

$$\frac{\partial \hat{h}}{\partial t} + \frac{\partial \hat{q}}{\partial x} = 0, \tag{15}$$

$$\begin{aligned}
&\frac{\partial \hat{q}}{\partial t} - \frac{9\delta}{2\,\mathrm{Re}}\frac{\partial^2 \hat{q}}{\partial x^2} + f_1\frac{\partial \hat{q}}{\partial x} + f_2\hat{q} + f_3\hat{h} + f_4\frac{\partial \hat{h}}{\partial x} + \frac{6\delta}{\mathrm{Re}\, h_s}\frac{\partial^2 \hat{h}}{\partial x^2} \\
&\quad - \frac{5}{6}\delta^2\,\mathrm{We}\, h_s\frac{\partial^3 \hat{h}}{\partial x^3} = 0,
\end{aligned} \tag{16}$$

where

$$f_1(x) = \frac{34\,\mathrm{Re} + 63\delta h_s'}{14\,\mathrm{Re}\, h_s},$$

$$f_2(x) = \frac{70 - 112\delta^2(h_s')^2 + 168\delta^2 h_s h_s'' - 72\delta\,\mathrm{Re}\, h_s' + 105\delta^2\zeta'' h_s + 70\delta^2\zeta' h_s' + 140\delta^2(\zeta')^2}{28\,\mathrm{Re}\,\delta h_s^2},$$

$$\begin{aligned}
f_3(x) = \frac{1}{84\,\mathrm{Re}\,\delta h_s^3}&(-504\delta^2 h_s h_s'' + 210\delta\cot\theta\zeta' h_s^3 + 216\,\mathrm{Re}\,\delta h_s' - 420 - 70\delta^3\,\mathrm{We}\,\mathrm{Re}\, h_s^3 h_s''' - 210h_s^3 - 840\delta^2(\zeta')^2 \\
&+ 672\delta^2(h_s')^2 - 420\delta^2 h_s'\zeta' - 70\delta^3\,\mathrm{We}\,\mathrm{Re}\, h_s^3\zeta''' - 315\delta^2\zeta'' h_s + 210\delta\cot\theta h_s^3 h_s'),
\end{aligned}$$

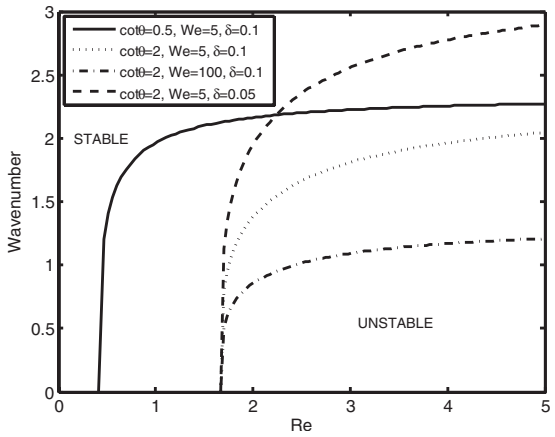

FIG. 2. Neutral stability curves for the even bottom case.

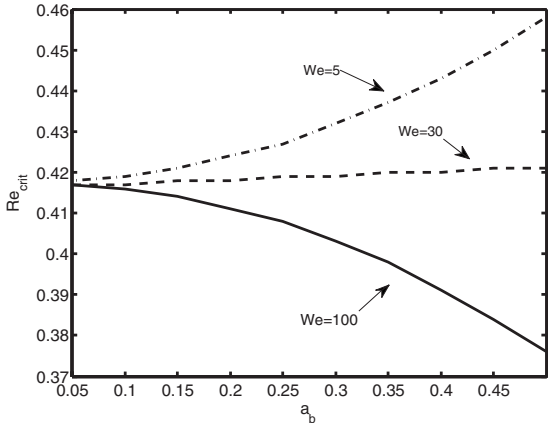

FIG. 3. Critical Reynolds number as a function of bottom amplitude with cot θ=0.5 and δ=0.1.

$$f_4(x) = \frac{-112\delta h_s' - 18\,\mathrm{Re} + 35\delta\zeta' + 35\cot\theta h_s^3}{14\,\mathrm{Re}\,h_s^2}.$$

We first validate our model against the even bottom case where $h_s(x) \equiv 1$. Here, we recover the well-established result that for instability $\mathrm{Re} > \frac{5}{6}\cot\theta$, and shown in Fig. 2 are neutral stability curves for the even bottom case. We note that for sufficiently steep inclinations the critical Reynolds number will remain $O(1)$, and thus our model will be second-order accurate.

For the case of an uneven bottom, the coefficients in Eqs. (15) and (16) are periodic functions. We thus apply Floquet–Bloch theory to conduct the stability analysis. Consequently, we represent the perturbations as Bloch-type functions having the form

$$\hat{h} = e^{\sigma t}e^{iKx}\sum_{n=-\infty}^{\infty}\hat{h}_n e^{i2\pi nx}, \quad \hat{q} = e^{\sigma t}e^{iKx}\sum_{n=-\infty}^{\infty}\hat{q}_n e^{i2\pi nx}.$$

The exponential factor containing the Bloch wavenumber K represents disturbances which interact with the periodic bottom topography via the equilibrium flow, which is represented by the Fourier series composed of its harmonics. Introducing the Bloch-type functions with truncated series into the perturbation equations yields an algebraic eigenvalue problem. In the case of small δ an approximate method of solution, making use of the analytical steady-state solution, can be employed. However, in the general case the algebraic eigenvalue problem must be solved numerically for the temporal growth rate $\Re(\sigma)$. In this way we can determine the critical Reynolds number for the onset of instability, and for supercritical flows we can compute the wavelength and speed of unstable disturbances.

Our results reveal that while the critical Reynolds number is independent of the Weber number for the even bottom case, in the presence of bottom topography the onset of instability is strongly influenced by the effect of surface tension. In Fig. 3 we present the distribution of the critical Reynolds number $\mathrm{Re}_{\mathrm{crit}}$ with the amplitude of the bottom undulations a_b for several values of We. It can be seen that increasing We has a destabilizing effect on the flow. It is also apparent that the entire $\mathrm{Re}_{\mathrm{crit}}$ distribution with respect to a_b lies either above or below the value corresponding to the even bottom case. In particular, for $\mathrm{We} \lesssim 30$ the $\mathrm{Re}_{\mathrm{crit}}$ values are larger than the value for $a_b=0$, while for We=100 the $\mathrm{Re}_{\mathrm{crit}}$ values are less than the value for $a_b=0$. Based on these results, the general indication is that bottom topography plays a stabilizing role for small to moderate Weber numbers, while for larger Weber numbers bottom unevenness tends to destabilize the flow.

In order to determine if varying the other parameters affects this conclusion, we concentrated on the cases having We=5 and We=100. With We=5 we found that for all the uneven bottom configurations considered, $\mathrm{Re}_{\mathrm{crit}}$ is larger than that for the even bottom. With We=100, however, we discovered that the effect of bottom topography on flow stability is dependent on δ. Examining the results in Fig. 4 it can be seen that for δ=0.05, $\mathrm{Re}_{\mathrm{crit}}$ increases with a_b, while for the larger δ values the opposite occurs. Lastly, in all of the cases considered we have observed that the $\mathrm{Re}_{\mathrm{crit}}$ distribution with respect to a_b still lies entirely above or below the value corresponding to the even bottom case. Thus, whether the role played by bottom topography is to stabilize or destabilize the flow depends not on the bottom amplitude, but rather on δ and We.

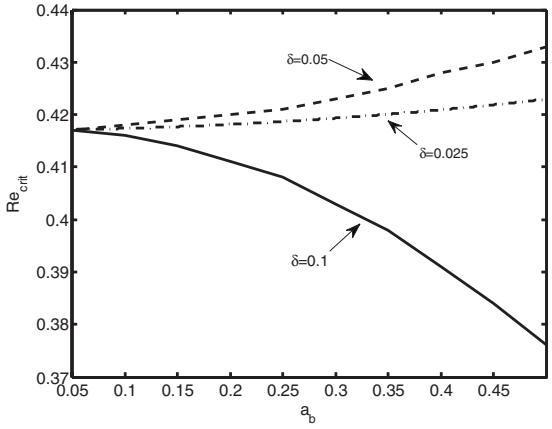

FIG. 4. Critical Reynolds number as a function of bottom amplitude with cot θ=0.5 and We=100.

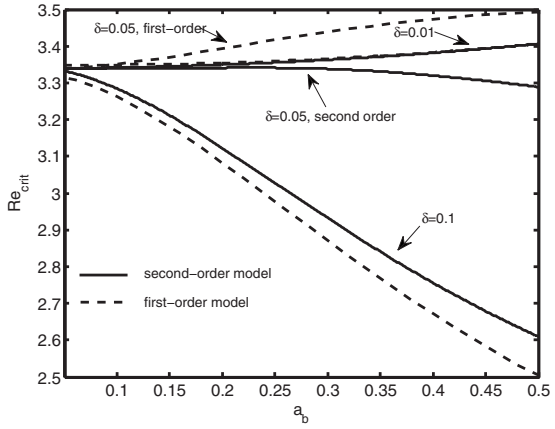

FIG. 5. Critical Reynolds number as a function of bottom amplitude with cot θ=4 and We=100.

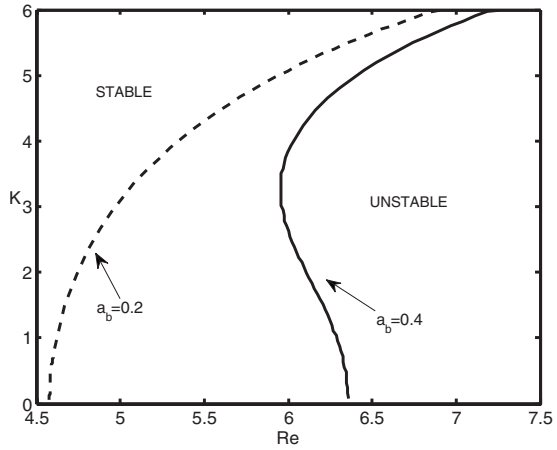

FIG. 7. Neutral stability curves for the case with cot θ=5, We=5, and δ=0.05.

Summarizing, based on our linear analysis we can make the following general conclusions. For weak to moderately strong surface tension bottom topography acts to stabilize the flow, while for stronger surface tension bottom topography destabilizes the flow provided that δ is sufficiently large. Since $\delta=H/\lambda_b$, increasing δ can be associated with shorter bottom wavelengths. The stabilizing influence of bottom topography combined with weak surface tension was also analytically obtained and experimentally verified by Wierschem *et al.*[22]

To illustrate the consequences of including second-order terms in our model, we next present results with and without these terms. In Fig. 5 it can be seen that the first-order hydrostatic model predicts that bottom topography stabilizes the flow for δ=0.05, while the second-order nonhydrostatic model yields the opposite conclusion. Further significant differences between the first- and second-order models are observed in Fig. 6 for δ=0.05 and δ=0.1.

Lastly, we focus on the wavelength of the unstable perturbations at the onset of instability. Examining the neutral stability curves presented in Fig. 7 it can be seen that for smaller values of a_b infinitely long wavelength perturbations are the first to become unstable. For larger a_b, however, the perturbations that first become unstable have finite wavelength. We have found that, in general, this dependence of the wavelength of unstable perturbations at the onset of instability on a_b is associated with sufficiently small values of δ and sufficiently large values of cot θ.

In Sec. IV we present a numerical method for solving the governing equations. Fully nonlinear numerical simulations will then be used to confirm some of the predictions made here.

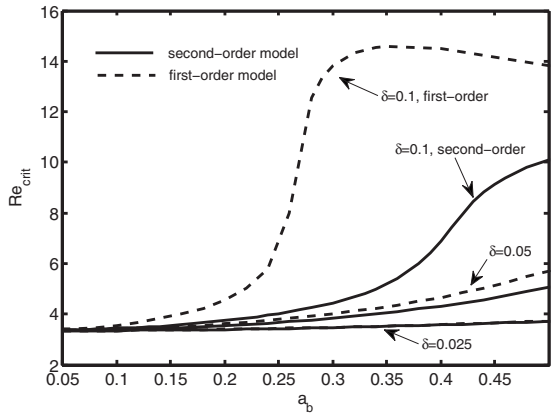

FIG. 6. Critical Reynolds number as a function of bottom amplitude with cot θ=4 and We=5.

IV. NUMERICAL SOLUTION PROCEDURE AND RESULTS

The instability of a particular equilibrium flow can be determined by gauging the evolution initiated by small disturbances. The development of the flow can be calculated by numerically solving the governing equations. The advantage of this approach is that it incorporates nonlinear interactions of the perturbations and thus captures the entire instability mechanism of the flow. Furthermore, for unstable flows the temporal evolution can be continued until the growth of the disturbances reaches saturation with the solution, then revealing the structure of the subsequent secondary flow. Such a numerical approach to nonlinear stability analysis has also been pursued by Kraneneburg,[34] Brook *et al.*,[35] Chang *et al.*,[36] Zanuttigh and Lamberti,[37] Balmforth and Mandre,[28] and Pascal and D'Alessio.[38]

For the purpose of a more effective presentation of the numerical method utilized to solve our problem, we first express the governing equations (12) and (13) in vector form as

$$\frac{\partial v}{\partial t}+\frac{\partial}{\partial x}f(v)=\Psi(v,x)+\chi\left(v,\frac{\partial v}{\partial x},\frac{\partial^2 v}{\partial x^2},\frac{\partial^3 v}{\partial x^3},x\right),$$

where

$$v=[h,q]^T,\quad f=\left[q,\frac{9}{7}\frac{q^2}{h}+\frac{5\cot\theta}{4\,\mathrm{Re}}h^2\right]^T,$$

$$\Psi = \left[0, \frac{5}{2\delta\,\mathrm{Re}}\left(h - \frac{q}{h^2}\right) - \frac{5\cot\theta\zeta' h}{2\,\mathrm{Re}} + \frac{5}{6}\delta^2\,\mathrm{We}\,\zeta''' h - \frac{15\delta\zeta'' q}{4\,\mathrm{Re}\,h} - \frac{5\delta(\zeta')^2 q}{\mathrm{Re}\,h^2}\right]^T,$$

and χ is an $\mathbb{R}^2$ vector with the first component being zero and the second component representing the derivative dependent source terms. In order to obtain numerical approximations to these equations, we march forward in time and advance the approximation from one time level to the next through a fractional-step splitting strategy. In particular, we first solve

$$\frac{\partial v}{\partial t} + \frac{\partial}{\partial x} f(v) = \Psi(v,x), \tag{17}$$

over a time step Δt, and then use the result as an initial condition to solve

$$\frac{\partial v}{\partial t} = \chi\left(v, \frac{\partial v}{\partial x}, \frac{\partial^2 v}{\partial x^2}, \frac{\partial^3 v}{\partial x^3}, x\right) \tag{18}$$

for the solution at the new time $t+\Delta t$. Equation (17) is a system of nonlinear hyperbolic conservation laws while dealing with Eq. (18), as we will see, reduces to solving a generalized one-dimensional diffusion equation. Solving Eq. (17) requires a specialized numerical scheme that is shock capturing and effectively eliminates spurious numerical oscillations while providing high-resolution results. Care must also be taken in dealing with the source term, $\Psi(v,x)$.

We solved Eq. (17) by employing a modified version of the high-resolution wave-propagation algorithm first introduced by LeVeque.[39] The modification has been proposed by Bale *et al.*[40] and consists of utilizing an eigenvector decomposition of flux differences instead of state variable differences. This method captures the balance between the source term and the flux gradient which is appropriate for cases when the solution grows slowly in time. The method is of finite-volume type which provides approximations to the cell average of the solution at a particular time level $t=t_n$ given by

$$V_i^n \approx \frac{1}{\Delta x}\int_{x_{i-1/2}}^{x_{i+1/2}} v(x,t_n)dx.$$

The cell average is updated at the next time level by considering a Riemann problem with states V_{i-1}^n and V_i^n centered at the cell edge $x_{i-1/2}$. The flux difference across the cell edge and the contribution of the source term are decomposed into waves based on the eigenvectors of an approximate Jacobian matrix of the flux, $A_{i-1/2}$, defined at the cell edge. In particular, we consider $A_{i-1/2}=f_v(\bar{V}_{i-1/2})$, where $\bar{V}_{i-1/2}$ is the average of V_{i-1}^n and V_i^n.

The combination of the flux difference across the cell boundary and the effect of the source term over the cell is decomposed as a linear expansion of the eigenvectors of the matrix $A_{i-1/2}$ as

$$f(V_i^n) - f(V_{i-1}^n) - \Delta x\psi(\bar{V}_{i-1/2}, x_{i-1/2}) = \sum_{m=1}^{2} \alpha_{i-1/2}^{(m)} r^{(m)}(\bar{V}_{i-1/2}) \equiv \sum_{m=1}^{2} \mathcal{Z}_{i-1/2}^{(m)}, \tag{19}$$

where $r^{(m)}(v)$, $m=1,2$ are the right eigenvectors of $A_{i-1/2}$ and the coefficients of the expansions are given by

$$\alpha_{i-1/2} = [r^{(1)}(\bar{V}_{i-1/2})|r^{(2)}(\bar{V}_{i-1/2})]^{-1}(f(V_i^n) - f(V_{i-1}^n) - \Delta x\psi(\bar{V}_{i-1/2}, x_{i-1/2})).$$

This decomposition provides the propagating f-waves, $\mathcal{Z}_{i-1/2}^{(m)}$, $m=1,2$ which are used to update the cell average at the subsequent time level. The updating formula is

$$V_i^{n+1} = V_i^n - \frac{\Delta t}{\Delta x}\left[\sum_{m:s_{i-1/2}^{(m)}>0} \mathcal{Z}_{i-1/2}^{(m)} + \sum_{m:s_{i+1/2}^{(m)}<0} \mathcal{Z}_{i+1/2}^{(m)}\right] - \frac{\Delta t}{\Delta x}[\tilde{F}_{i+1/2} - \tilde{F}_{i-1/2}],$$

where

$$\tilde{F}_{i-1/2} = \frac{1}{2}\sum_{m=1}^{2} \mathrm{sgn}(s_{i-1/2}^{(m)})\left(1 - \frac{\Delta t}{\Delta x}|s_{i-1/2}^{(m)}|\right)\tilde{\mathcal{Z}}_{i-1/2}^{(m)}.$$

Here $\tilde{\mathcal{Z}}_{i-1/2}^{(m)}$ are limited versions of the f-waves necessary for the method to provide oscillation-free results. The speeds of propagation of the f-waves are denoted by $s_{i-1/2}^{(m)}$ and are obtained from the eigenvalues of the Jacobian matrix of the flux vector evaluated at $v=\bar{V}_{i-1/2}$.

Solving Eq. (17) handles the advective nature of the solution, whereas solving Eq. (18) in the second step captures the viscous nature of the solution. This reduces to solving the generalized one-dimensional nonlinear diffusion equation having the form

$$\frac{\partial q}{\partial t} = \frac{9\delta}{2\,\mathrm{Re}}\frac{\partial^2 q}{\partial x^2} + \frac{q}{7h}\frac{\partial q}{\partial x} + S_1\frac{\partial q}{\partial x} + S_0 q + S,$$

where the functions S, S_0, and S_1 are easily obtainable. Since h is known from the first step and remains constant during the second step, the functions S, S_0, and S_1 are known. Discretizing the above equation using the Crank–Nicolson scheme, imposing periodicity conditions, and using the output from the first step as an initial condition leads to a nonlinear system of algebraic equations which was solved iteratively using a robust algorithm which takes advantage of the structure and sparseness of the resulting linearized system.

We employed the numerical method to solve the governing equations on a periodic spatial domain of size L and calculate the evolution of a perturbed equilibrium flow. The initial state was taken to be $q=1$, while for h we used the numerically generated steady-state solution. The truncation error associated with this solution served as a wide-band perturbation of small amplitude imposed on the steady flow. The length of the periodic computational domain, L, is an artificial parameter in our problem. Experimentation was performed in order to determine the effect of this parameter, since its prescribed value restricts the wavelength of the per-

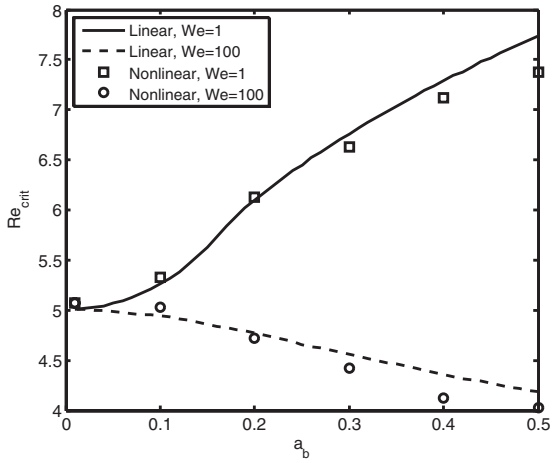

FIG. 8. Critical Reynolds numbers for $\delta=0.07$ and cot $\theta=6$ obtained using the linear analysis and nonlinear simulations.

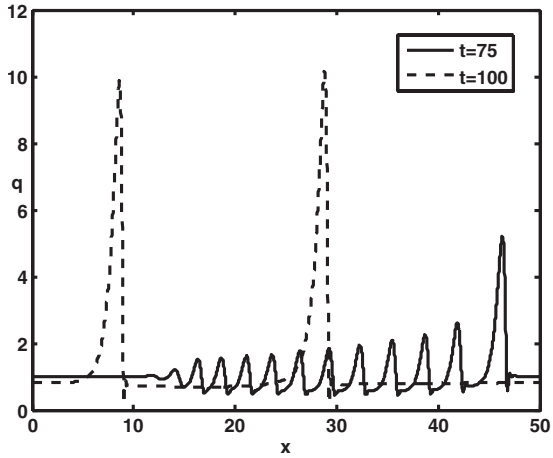

FIG. 10. The evolution of the q distribution for the case with Re=3, cot $\theta=1$, We=5, $a_b=0.2$, and $\delta=0.1$ on a computational domain of length $L=50$.

turbations imposed on the flow and thus affects the structure of the interfacial waves generated in unstable flows. In order to track the evolution of the perturbations, we monitored the spatial distribution of q where perturbations were measured by the variation of the solution from the constant state. Typical computational parameters used in our simulations included a uniform grid spacing of $\Delta x=0.01$ and a time step of $\Delta t=0.002$. For cases with surface tension the time step had to be decreased in accordance with the value of We due to the higher spatial derivative appearing in the surface tension term. Contrasted in Fig. 8 are the critical Reynolds numbers as obtained by the linear stability analysis and the nonlinear simulations. From the diagram we see that the values predicted by the linear analysis agree closely with those determined by the simulations. The apparent trend is that for small a_b the nonlinear simulations yield slightly larger values for $\mathrm{Re}_{\mathrm{crit}}$ than those calculated by the linear analysis, while for larger a_b the opposite was found.

The progression of an unstable flow, as described by our results, consists of the general phases observed for film flows[41] and inclined flows[2,42] along even surfaces. We next present some simulations illustrating the evolution of interfacial waves for the supercritical case having Re=3, cot $\theta=1$, $a_b=0.2$, and $\delta=0.1$. Figures 9 and 10 deal with We=5, while Fig. 11 is for We=100. The corresponding case with no surface tension is portrayed in Fig. 12. Figure 9 illustrates the evolution on a domain having $L=20$. With the passage of time the growth in amplitude of the perturbation saturates and the wavefronts steepen. Wave coarsening, a subharmonic instability whereby bores traveling with different speeds combine to form a wave pattern having fewer but taller bores, then occurs and gives rise to two solitary humps separated by a fixed distance. This pattern persists for all $t>200$. Wave coarsening resulting in two solitary humps was also observed on the larger computational domain having $L=50$ shown in Fig. 10. Increasing the Weber number to 100 also results in an ultimate wave pattern consisting of two solitary humps as illustrated in Fig. 11. We note that for larger We, the amplitudes of the waves are noticeably smaller and the time required for the wave coarsening process is significantly longer. For the cases with surface tension, plotted in Figs. 9–11, the solitary humps are accompanied by

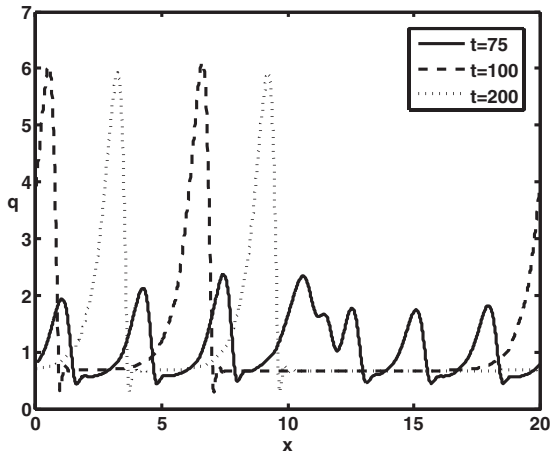

FIG. 9. The evolution of the q distribution for the case with Re=3, cot $\theta=1$, We=5, $a_b=0.2$, and $\delta=0.1$ on a computational domain of length $L=20$.

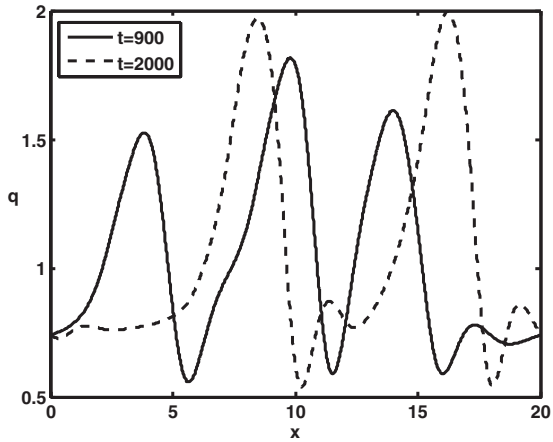

FIG. 11. The evolution of the q distribution for the case with Re=3, cot $\theta=1$, We=100, $a_b=0.2$, and $\delta=0.1$ on a computational domain of length $L=20$.

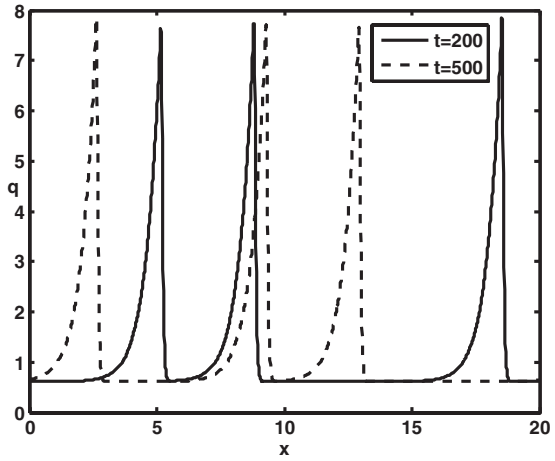

FIG. 12. The evolution of the q distribution for the case with Re=3, cot θ=1, We=0, a_b=0.2, and δ=0.1 on a computational domain of length L=20.

front-running bow waves and the features displayed are similar to those reported by Ruyer-Quil and Manneville.[33] In Fig. 12 surface tension is turned off and this time wave coarsening results in a wave pattern consisting of three peaks with no front-running waves. For turbulent flows, Chang *et al.*[36] claimed that an interruption in wave coarsening is a consequence of the artificially imposed periodicity and that if the computational domain is sufficiently long wave coarsening continues to completion, whereby the waves coalesce and ultimately form a single solitary wave profile. Balmforth and Mandre[28] have explored this destabilization of wave trains of multiple waves quite thoroughly. Our results agree, in principle, with their conclusion which is that there is a critical distance between peaks such that if this distance is sufficiently large then coarsening will be interrupted.

V. CONCLUDING REMARKS

This paper solved the problem of laminar flow down an uneven surface for a wide range of inclinations. In particular, the impact of periodically varying bottom topography on the stability of the flow was investigated. The key contributions offered by this work are threefold. These include a mathematical model based on the weighted residual strategy first proposed by Ruyer-Quil and Manneville[9] for an even bottom, which we have extended to account for bottom topography. In addition, an efficient and successful numerical solution procedure, founded on the recent algorithm advanced by Bale *et al.*,[40] has been provided to simulate the flow. Lastly, the combined effect of surface tension and wavy bottom topography for Weber numbers ranging from 0 to 100 has been quantified.

The impact of retaining second-order terms in our model was also assessed. It was found that in certain cases the second-order terms led to significant differences in the influence that bottom topography has on the stability of the flow. Thus, the second-order nonhydrostatic model proposed in this study represents an important improvement over first-order hydrostatic models.

Although no direct comparisons with experiments or direct numerical simulations have been made, indirect comparisons can be inferred. For example, for the case of an even bottom with surface tension, the results obtained by the linear stability analysis are in full agreement with those of Ruyer-Quil and Manneville[33] which in turn agree with experiments reported by Liu *et al.*[10] and the direct numerical simulations carried out by Ramaswamy *et al.*[11] For the case of a wavy bottom with weak surface tension, our predictions are consistent with the recent results of Wierschem *et al.*[22] which have been supported by their experiments.

The main conclusion of this research is that, in general, for weak to moderate surface tension, bottom topography acts to stabilize the flow. However, for stronger surface tension, bottom topography can destabilize the flow provided that the wavelengths of the bottom undulations are sufficiently short. While the stabilizing effect of bottom topography on inclined flows has been previously reported by Wierschem *et al.*[22] for weak surface tension and Balmforth and Mandre[28] for zero surface tension, the potentially destabilizing combined effect of bottom topography and stronger surface tension has not been previously discovered, at least to our knowledge.

ACKNOWLEDGMENTS

Financial support for this research was provided by the Natural Sciences and Engineering Research Council of Canada.

[1] S. Alekseenko, V. Nakoryakov, and B. Pokusaev, "Wave formation on a vertical falling liquid film," AIChE J. **31**, 1446 (1985).
[2] P. Julien and D. Hartley, "Formation of roll waves in laminar sheet flow," J. Hydraul. Res. **24**, 5 (1986).
[3] T. B. Benjamin, "Wave formation in laminar flow down an inclined plane," J. Fluid Mech. **2**, 554 (1957).
[4] C.-S. Yih, "Stability of liquid flow down an inclined plane," Phys. Fluids **6**, 321 (1963).
[5] J. Liu, J. D. Paul, and J. P. Gollub, "Measurements of the primary instabilities of film flows," J. Fluid Mech. **250**, 69 (1993).
[6] V. Y. Shkadov, ""Wave conditions in flow of thin layer of a viscous liquid under the action of gravity," Izv. Akad. Nauk SSSR, Mekh. Zhidk. Gaza **1**, 43 (1967).
[7] T. Prokopiou, M. Cheng, and H.-C. Chang, "Long waves on inclined films at high Reynolds number," J. Fluid Mech. **222**, 665 (1991).
[8] H. Uecker, "Approximation of the integral boundary layer equation by the Kuramoto–Sivashinsky equation," SIAM J. Appl. Math. **63**, 1359 (2003).
[9] C. Ruyer-Quil and P. Manneville, "Improved modeling of flows down inclined planes," Eur. Phys. J. B **15**, 357 (2000).
[10] J. Liu, B. Schneider, and J. P. Gollub, "Three-dimensional instabilities of film flows," Phys. Fluids **7**, 55 (1995).
[11] B. Ramaswamy, S. Chippada, and S. W. Joo, "A full-scale numerical study of interfacial instabilities in thin-film flows," J. Fluid Mech. **325**, 163 (1996).
[12] D. J. Benney, "Long waves on liquid films," J. Math. Phys. **54**, 150 (1966).
[13] B. Hunt, "Newtonian fluid mechanics treatment of debris flows and avalanches," J. Hydraul. Eng. **120**, 1350 (1994).
[14] C.-O. Ng and C. C. Mei, "Roll waves on a shallow layer of mud modelled as a power-law fluid," J. Fluid Mech. **263**, 151 (1994).
[15] Q. Liu, L. Chen, J. Li, and V. Singh, "Roll waves in overland flow," J. Hydrol. Eng. **10**, 110 (2005).
[16] S. Montes, *Hydraulics of Open Channel Flow* (ASCE, Reston, VA, 1998).
[17] Y. Y. Trifonov, "Viscous liquid film flows over a periodic surface," Int. J. Multiphase Flow **24**, 1139 (1998).

[18]C. Heining, V. Bontozoglou, N. Aksel, and A. Wierschem, "Nonlinear resonance in viscous films on inclined wavy planes," Int. J. Multiphase Flow **35**, 78 (2009).
[19]H. Tougou, "Long waves on a film flow of a viscous fluid down an inclined uneven wall," J. Phys. Soc. Jpn. **44**, 1014 (1978).
[20]R. Usha and B. Uma, "Long waves on a viscoelastic film flow down a wavy incline," Int. J. Non-Linear Mech. **39**, 1589 (2004).
[21]L. A. Davalos-Orozco, "Nonlinear instability of a thin film flowing down a smoothly deformed surface," Phys. Fluids **19**, 074103 (2007).
[22]A. Wierschem, C. Lepski, and N. Aksel, "Effect of long undulated bottoms on thin gravity-driven films," Acta Mech. **179**, 41 (2005).
[23]M. Vlachogiannis and V. Bontozoglou, "Experiments on laminar film flow along a periodic wall," J. Fluid Mech. **457**, 133 (2002).
[24]Y. Y. Trifonov, "Stability and nonlinear wavy regimes in downward film flows on a corrugated surface," J. Appl. Mech. Tech. Phys. **48**, 91 (2007).
[25]Y. Y. Trifonov, "Stability of a viscous liquid film flowing down a periodic surface," Int. J. Multiphase Flow **33**, 1186 (2007).
[26]R. E. Khayat and K. T. Kim, "Thin-film flow of a viscoelastic fluid on an axisymmetric substrate of arbitrary shape," J. Fluid Mech. **552**, 37 (2006).
[27]A. Oron and C. Heining, "Weighted-residual integral boundary-layer model for the nonlinear dynamics of thin liquid films falling on an undulating vertical wall," Phys. Fluids **20**, 082102 (2008).
[28]N. J. Balmforth and S. Mandre, "Dynamics of roll waves," J. Fluid Mech. **514**, 1 (2004).
[29]R. F. Dressler, "Mathematical solution of the problem of roll waves in inclined open channels," Commun. Pure Appl. Math. **2**, 149 (1949).
[30]D. Needham and J. Merkin, "On roll waves down an open inclined channel," Proc. R. Soc. London, Ser. A **394**, 259 (1984).
[31]C. Ruyer-Quil and P. Manneville, "Modeling film flows down inclined planes," Eur. Phys. J. B **6**, 277 (1998).
[32]J.-J. Lee and C. C. Mei, "Stationary waves on an inclined sheet of viscous fluid at high Reynolds and moderate Weber numbers," J. Fluid Mech. **307**, 191 (1996).
[33]C. Ruyer-Quil and P. Manneville, "Further accuracy and convergence results on the modeling of flows down inclined planes by weighted-residual approximations," Phys. Fluids **14**, 170 (2002).
[34]C. Kranenburg, "On the evolution of roll waves," J. Fluid Mech. **245**, 249 (1992).
[35]B. S. Brook, T. J. Pedley, and S. A. Falle, "Numerical solutions for unsteady gravity-driven flows in collapsible tubes: Evolution and roll-wave instability of a steady state," J. Fluid Mech. **396**, 223 (1999).
[36]H.-C. Chang, E. A. Demekhin, and E. Kalaidin, "Coherent structures, self-similarity and universal roll wave coarsening dynamics," Phys. Fluids **12**, 2268 (2000).
[37]B. Zanuttigh and A. Lamberti, "Roll waves simulation using shallow water equations and weighted average flux method," J. Hydraul. Res. **553**, 610 (2002).
[38]J. P. Pascal and S. J. D. D'Alessio, "Instability of power-law fluid flows down an incline subjected to wind stress," Appl. Math. Model. **31**, 1229 (2007).
[39]R. J. Leveque, "Wave propagation algorithms for multi-dimensional hyperbolic systems," J. Comput. Phys. **131**, 327 (1997).
[40]D. S. Bale, R. J. Leveque, S. Mitran, and J. A. Rossmanith, "A wave propagation method for conservation laws and balance laws with spatially varying flux functions," SIAM J. Sci. Comput. (USA) **24**, 955 (2003).
[41]H.-C. Chang, "Wave evolution on a falling film," Annu. Rev. Fluid Mech. **26**, 103 (1994).
[42]R. R. Brock, "Development of roll-wave trains in open channels," J. Hydr. Div. **95**, 1401 (1969).